# Negative correlation of doping and conductivity in $Ln_{1-x}M_xCr_{0.9}Ni_{0.1}O_3$ (Ln = La and/or Nd; M = Sr and/or Ca; x≤0.25) perovskites prepared by combustion synthesis as anode materials for SOFCs

**L. Ortega-San-Martín[a], A. Morán-Ruiz[b], A. Wain-Martin[b], K. Vidal[b], A. Larrañaga[b], M.A. Laguna-Bercero[c] and M.I. Arriortua[b,d]**

[a]Departamento de Ciencias, Sección Química, Pontificia Universidad Católica del Perú (PUCP), Av. Universitaria 1801, Lima 32, Perú.

[b]Facultad de Ciencia y Tecnología, Universidad del País Vasco/Euskal Herriko Unibertsitatea (UPV/EHU), Sarriena s/n, 48940 Leioa, Spain.

[c]CSIC-Universidad de Zaragoza, Instituto de Ciencia de Materiales de Aragón (ICMA), Pedro Cerbuna 12, 50009 Zaragoza, Spain.

[d]BCMaterials, Parque Tecnológico de Zamudio, Ibaizabal Bidea, Edificio 500- Planta 1, 48160 Derio, Spain.



**Abstract**:

A series of chromite perovskites with the general formula $Ln_{1-x}M_xCr_{0.9}Ni_{0.1}O_3$ (Ln = La and/or Nd; M = Sr and/or Ca; x≤0.25) has been prepared by three combustion synthesis routes using a different fuel each time: glycine, urea and sucrose. In order to isolate the effect of divalent dopant concentration from the A cation steric effects, the whole group has a fixed mean A cation radius, $\langle r_A \rangle \approx 1.22$ Å, and cation size disorder, $\sigma^2(r_A) \approx 0.0001$ Å$^2$, but variable doping x. Their crystal structure, microstructure, electrical properties and expansion coefficients have been investigated on the basis of their possible use as anode materials for intermediate temperature solid oxide fuel cells (SOFC). Important dependences of the cell parameters, grain size, the expansion coefficients and the conductivity with x and the used fuel are observed. The most

interesting feature of these oxides is their negative dependence of the conductivity with x under $H_2$ atmosphere: smaller conductivity is observed when doping is increased, which has not been reported before.

**Keywords:** Chemical Synthesis; Electrical Conductivity; SOFC; Anode; A-site.

---

* Corresponding Authors: Karmele Vidal, María Isabel Arriortua, Luis Ortega-San Martin
e-mail: karmele.vidal@ehu.es, maribel.arriortua@ehu.es, lortegas@pucp.edu.pe
Phone number: 946015984; Fax number: 946013500.

## 1. Introduction

The research to find new or to improve the most commonly used materials for Solid Oxide Fuel Cells (SOFC) is still a important field in materials science[1]. Recent reviews suggest that one of the most active area is the study of SOFC anodes given that the operation of commercial SOFC devices is strongly dependent on the behaviour of this electrode which is in contact with the fuel (and all its impurities)[2]. The number of materials studied as possible anodes is huge and, among them, perovskites have also gained attraction due to their good catalytic properties, high ionic and electrical conductivities, and their chemical and thermal stabilities at high temperatures.

The main concern for current nickel-yttria stabilized zirconia cermet anodes is that they are unable to work efficiently with hydrocarbon fuels at intermediate operating temperature range (600-800°C) due to their sulfur content and also as a consequence of carbon deposition.[3] Hence, there is still a demand for the development of alternate anode materials with improved tolerance towards carbon deposition and sulfur poisoning to improve the fuel flexibility and efficiency of SOFCs.

Oxide-perovskites have been widely studied as possible cathode electrodes for a long time due to their stability under oxidising conditions, but in recent years their possible use as anodes is under consideration[4–8]. Perovskite based materials have tuneable oxygen ion vacancies depending on composition, temperature, and surrounding crystalline environment. This results in mixed ionic and electronic conductivity (MIEC), which is highly beneficial for SOFC anodes, as it allows for the electrode reaction to occur on the whole surface on the electrode material, improving electrochemical properties. Given that the perovskite structure can accommodate almost all the elements in the periodic table, good catalytic properties are also accessible.

Among oxide perovskites, there are not many stable compounds under reducing conditions. Chromites, however, are among the few and they have been thoroughly investigated as SOFC-interconnectors because they are reasonably stable in both oxidising and reducing atmospheres[9]. Consequently, their potential to be used as SOFC-anodes is also being investigated. From the thermodynamic point of view, chromites are expected to react with the common YSZ electrolyte but in practice, this only occurs to a great extent at temperatures above the operation ones (that is, higher than 1000ºC)[10].

When a material is evaluated as a SOFC component, it is also important to consider its preparation costs. Perovskites are usually prepared at high temperatures so another important field of research is aimed at reducing energy consumption of the synthesis[11]. To synthesize nano-size powders with high specific surface area, combustion methods are of great importance: they use low cost materials, tend to be fast processes and usually result in oxides with submicrometer particle sizes (the large production of gases inhibits particle size growth)[12]. In this type of synthesis, the combustion velocity, the choice of the fuel type and its amount are very important factors that influence the combustion and, in turn, the final properties of the obtained powder[13].

The effect of the combustion fuel on the electrochemical properties of SOFC materials has been investigated recently, for both single fuels and fuel mixtures. Nevertheless, good explanations about the effect of the combustion fuel are scarce.[14].

In this study, we investigate two effects: (i) the variation of the doping level x and (ii) the use of different fuels (glycine, urea and sucrose) during the synthesis by the combustion method in the structure and electrical properties of a series of new chromite perovskites with the formula $Ln_{1-x}M_xCr_{0.9}Ni_{0.1}O_3$ (Ln = La and/or Nd; M = Sr and/or

Ca; x≤0.25). To avoid the interplay of different A-site variables in their properties the mean ionic radius $<r_A>$ (1.22 Å) and the cation size disorder $\sigma^2(r_A)$ (0.0001 $Å^2$) have been kept constant. Low disorder (quantified as $\sigma^2(r_A) = <r_A^2> - <r_A>^2$) has been selected from previous studies showing that the higher the disorder the lower the performance of the oxides irrespective their field of application.[15–19] On the other hand, the chemical compositions have been selected bearing in mind the maximum solubility of calcium and strontium in chromites as reported in the literature and considering that the presence of strontium improves their stability under low oxygen pressures typically found in SOFC anodes[10]. X-ray powder diffraction (XRD), scanning electron microscopy (SEM), electrical measurements and thermal expansion studies have been also carried out.

## 2. Experimental

### *2.1. Powder preparation*

$Ln_{1-x}M_xCr_{0.9}Ni_{0.1}O_3$ samples were prepared by combustion synthesis using $La(NO_3)_3.6H_2O$ (>99%), $Nd(NO_3)_3.6H_2O$ (99.9%), $Sr(NO_3)_2$. (99.99%), $Ca(NO_3)_2$. $H_2O$ (99.997%), $Ni(NO_3)_2.6H_2O$ (99.999%) and $Cr(NO_3)_3$ (>99%) as metal precursors and glycine, urea and sucrose (all from Aldrich, >99%) as combustion fuels. The prepared compositions, together with their mean ionic radius, $<r_A>$, and A cation size disorder, $\sigma^2(r_A)$, are summarised in Table 1.

Table 1

The metal nitrates were dissolved in distilled water. The solutions (dissolved metal nitrates) were mixed in a glass beaker, which was placed on a hot plate, under constant stirring, to evaporate excess water. Then, the glycine, urea or sucrose was added to obtain a fuel/oxidizer molar ratio of 1. The resulting viscous liquid started autoignition

just after placing the glass beaker directly onto a preheated plate (at 350°C). The obtained powders were calcined at 800°C for 2 h to remove the carbon residues and, after that, these samples were pressed at 45 MPa to form 13 mm diameter pellets by a manual hydraulic press and calcined in air between 1100 and 1200ºC for 10 hours at each temperature until pure samples were obtained.

*2.2. Characterization techniques*

The structural analysis was performed using laboratory X-ray diffraction (XRD). Room temperature XRD data were collected from 15 to 90° in 2θ with an integration time of 500 s/0.026° step using a Philips X'Pert-PRO X-ray diffractometer using copper Kα radiation without Ni-filter and a PIXcel solid state detector (active length in 2θ 3.347º). A fixed divergence and antiscattering slit giving a constant volume of sample illumination were used. The crystal structure was refined by the Rietveld method using the GSAS software package[20] and EXPGUI interface[21].

All metal contents were determined by inductively coupled plasma atomic emission spectroscopy (ICP-AES) on a Horiba Yobin Yvon Activa spectrophotometer. For this purpose, samples were dissolved using a mixture of $HNO_3$ and HCl for two days to obtain a clear and measurable solution.

Prior to bulk conductivity and dilatometry measurements pellets of the as-synthesised powders were sintered at 1350°C for 10 hours and, subsequently, cut into bars. The bulk density of each sample was estimated by measuring the mass and the dimensions of the bars. DC conductivity measurements were performed under pure $H_2$ by the four-point DC method from 800 to 400°C using a VSP potenciostat controlled by PC using Lab Windows/CVI field point system. Electrical contacts were made using Pt wires and Pt paste placed over whole end faces ensuring a homogeneous current flow.

Prior to the start of the measurements, each oxide was kept at 800ºC for 12 h under flowing $H_2$ at a rate of 120 ml/min (oxygen partial pressure nearly $10^{-21}$ atm). Conductivity data were corrected considering the experimental density values (all around 85% of the theoretical (X-ray) density).

Thermal expansion coefficients were measured from room temperature to 950ºC under air with a heating rate of 5ºC.min$^{-1}$ using a Unitherm Model 1161 dilatometer. Morphologies of the as-synthesised powder samples and the sintered pellets were observed using a scanning electron microscope (JEOL JSM-7000F). Secondary electron images were taken at 20 kV and $1.1.10^{-11}$ A.

## 3. Results and discussion

### *3.1. Structural Study*

Room temperature X-ray diffraction patterns of all as-synthesised oxide perovskites are shown in Figure 1. The patterns reveal that all the samples are single-phase and no impurities are detected within the resolution limits of the used technique.

Figure 1

Results from chemical analyses, presented in Table 2, show a good agreement between the analysed chemical compositions of the prepared powders and the nominal compositions.

Table 2

Rietveld fits to the powder X-ray diffraction data were carried out using the orthorhombic (*Pnma*) space group, the same observed for the parent $LaCrO_3$ phase at room temperature[22], considering the nominal composition in the different sites of the crystal structure. Only three independent thermal parameters were used in the

refinements (one for the A-site cations, another for the B-site ones and a final one for all the oxygen atoms). Graphs of the Rietveld fits to all the oxides prepared by urea combustion are shown in Figure 2. Fits to the glycine and sucrose fuel-samples are shown in Figures S1 and S2 of the supplementary information, respectively.

Figure 2

Figures S1 and S2

The variation of the unit cell parameters and cell volume with doping (x) is shown in Figure 3. As it can be observed, there is a systematic decrease in volume with increasing divalent dopant content. This behavior cannot be associated with changes in the A position because the variables that influence lattice volume, such as the A-site mean ionic radius $<r_A>$ and the A-site disorder[23], have been kept constant throughout the series. Therefore, the observed decrease of the lattice parameters can be only associated with the reduction of the B-site (chromium and nickel) mean ionic radii ($<r_B>$) as a consequence of their oxidation with the increase of the doping level x (the ionic radii in octahedral coordination of Cr and Ni decrease from $r_{(Cr3+)}$ = 0.615 Å and $r_{(Ni2+)}$ = 0.69 Å to $r_{(Cr4+)}$ = 0.55 Å, and $r_{(Ni3+)}$ = 0.56 Å, respectively)[24].

Figure 3

The structural parameters, atomic distances and R factors obtained by Rietveld refinement to the X-ray data of all the compounds obtained using the different fuels are displayed in Tables S1 to S3 of the supplementary information. According to our data, there are not many structural variations along the series with doping apart from the compression of the unit cell, as expected.

The crystal structure of the oxides was also studied after the conductivity measurements that were carried out under hydrogen atmosphere in order to establish the stability of the samples. It is interesting to note that the room temperature XRD data

showed that none of the samples degraded and all were single phase after the treatment but with a different crystal structure: data were fitted to a *R*-3*c* distorted perovskite. This indicates that the oxides retain the high temperature phase of the parent LaCrO3 which experiments a *Pnma* → *R*-3*c* phase transition above 250ºC.[22] This higher symmetry structure is probably a result of the rearrangement of the atoms that resulted from the oxygen loss at temperatures between 400-800ºC. Nevertheless, the initial crystal structure is fully recovered after the oxides are heated again in air at 800ºC, as shown in Figure 4 for the x=0.1 oxide prepared using sucrose as the fuel. No impurities are observed after this cycle which further supports that these oxides are thermally stable as expected for anode perovskites.

Figure 4

*3.2. Morphological study*

Representative SEM micrographs of the powder samples obtained by the combustion method using glycine, urea and sucrose as fuels after final calcination (as-synthesised powders) are shown in Figure 5.

Figure 5

These powders are composed of agglomerates formed by very small size particles. The average size of the grains calculated by direct SEM observation ranges from 200-250 nm observed for the x = 0.10 oxide prepared using glycine as fuel to 550-600 nm observed for the x=0.25 phase prepared using sucrose. It is interesting to note that the average particle size slightly increases with x irrespective of the synthesis method, being the x=0.25 oxides the ones that show the biggest grain sizes.

Usually, smaller crystallite sizes are formed when the combustion temperature is not very high and, specially, when a large volume of gases is evolved because this further enhances the dissipation of heat and limits the inter-particle contact, preventing grain

growth. Fuel comparisons[13,25,26] in the literature, however, are not definitive regarding to which fuel results in smaller particles mainly because each author uses different fuel to oxidiser ratios, which has a strong influence on the combustion temperature, so those results are not easily comparable. In the present case, our results indicate that glycine and urea combustion yield smaller particles than sucrose probably because non-nitrogen containing fuels are not as efficient dissipating the combustion temperature than the nitrogen ones.

On the other hand, the increase of grain size with x can be related to the calcium content in the phases. Several studies have shown that the addition of calcium to $LaCrO_3$ allows the formation of a transient liquid phase due to the formation of $CaCrO_4$, specially above 1150ºC, resulting in sintered microstructures with bigger particle sizes and denser ceramics[27],[28].

After sintering at 1350ºC in air for 10h the trends in particle sizes are maintained, as observed in the SEM images shown in Figure 6: the higher the x (calcium content) the biggest the particle sizes. As expected, this also resulted in denser materials with x: from the lowest to the highest doping, the relative densities increased from 60 to 88%, from 76 to 95% and from 70 to 92% of the theoretical XRD-values for the perovskites synthesized using glycine, urea and sucrose, respectively.

Figure 6

Figure 6 also shows that, after sintering, all oxides present bigger particle sizes compared to the as-synthesised powders, which is an expected result, but the increase is dependent on the synthesis method, being the samples prepared by the urea combustion process the ones that show the biggest increase (near tenfold for the x=0.25 oxide). Figure 7 summarises the observed tendencies. This difference in the sintering behavior is probably a result of the different agglomeration that result from the combustion. The

better sinterability of the powders obtained using urea as fuel seems to indicate that the as-synthesized powders presented softer agglomerates which could be broken during cold-pressing to enhance number of contact points, as pointed out before[29].

Figure 7

*3.3. Electrical conductivity study*

The total electrical conductivity, σ, measured under $H_2$ atmosphere of all the sintered $Ln_{1-x}M_xCr_{0.9}Ni_{0.1}O_3$ perovskites as function of doping level x from 400 to 800ºC is shown in Figure 8a-c. A summary of the data at 800ºC for all the studied compounds appears in Figure 8d.

Figure 8

It can be clearly seen that the conductivity is strongly dependent on both the preparation route and the doping level. In all cases the oxides prepared by the urea combustion route show higher conductivity values than the glycine and sucrose oxides. It is interesting to note that the maximum conductivity values of the glycine and urea samples with x=0.1 and 0.15 are similar (in some cases higher) to previously reported values of other $Ln_{1-x}A'_xCr_{1-y}M_yO_{3-d}$ compounds at low oxygen partial pressures[30–33] and they are also above the minimum of 1 $Scm^{-1}$ expected for an oxide anode[34]. The sucrose samples, however, show conductivity values that are roughly an order of magnitude smaller and below those expected for anode applications.

The most important feature of the electrical behaviour of these samples is, however, the conductivity dependence on the doping value x. As observed, it follows the opposite trend that would be expected for these oxides: the conductivity decreases as the doping increases and this occurs irrespective of the synthesis process followed. This is interesting because, under air, this type of oxides show a p-type conductivity mainly based on the hoping process between $Cr^{4+}$ and $Cr^{3+}$ (together with some $Ni^{2+}$ – $Ni^{3+}$

exchange, in this case) and the conducting mechanism when x increases is well known: as the alkaline-earth ions are introduced in the A-site to substitute the rare earth ions the concentration of electronic holes (mainly $Cr^{4+}$, but also some $Ni^{3+}$ in the present case) increases to compensate for the smaller oxidation state of the new ions and, as a consequence, the same occurs to the p-type conductivity[35]. Under low oxygen partial pressures the formation of oxygen vacancies overrides this compensation mechanism and causes a strong reduction on the amount of holes (two $Cr^{4+}$ ions reduce to $Cr^{3+}$ in order to compensate for every $O^{2-}$ ion that leaves the lattice) and this is why, in this type of oxides, conductivity under reducing conditions is always smaller than under oxidizing conditions.[30–32,35–39] Nevertheless, if the conductivity of these oxides remained as p-type the same trend (increase of electrical conductivity) should be observed with increasing x (or y) as it has been reported in many of the previous studies of $A_{1-x}A'_xCr_{1-y}M_yO_3$ chromites.[31,32,37,39] However, we observe exactly the opposite behavior in all our cases irrespective of the synthesis process which indicates that this behavior is an intrinsic characteristic of the present oxides.

A thorough search of similar chromites in the literature has revealed that this behavior is, however, not that uncommon. In fact, it is observed in all calcium doped chromites when sufficiently low oxygen pressures are applied[30,37,38] although, to our surprise, none of the authors of the previous works have paid special attention to that fact. It was Karim and Aldred[35] who realized that, in the $La_{1-x}Sr_xCrO_3$ system with $0 \leq x \leq 0.4$ , the higher the doping the bigger was the reduction of the conductivity with the reduction of oxygen partial pressure ($pO_2$). But given that they did not plotted the evolution of the conductivity with x at different temperatures they did not notice that the trend observed under air (higher $\sigma$ with x) did not completely hold at very low $pO_2$. More recent works pointed out that the higher the doping the higher was the amount of

vacancies formed at low $pO_2$ but none paid attention to the changes that were occurring with conductivity although in the case of the $La_{1-x}Ca_xCrO_3$ samples studied by Yasuda in 1993 their fit to their pressure dependence of the conductivity clearly showed that the trend would be reverted at very low $pO_2$, as observed in our case.[30] This change in behavior at low $pO_2$ compared to the one observed in air can also be sensed from the data of manganites such as $La_{1-x}Sr_xMnO_3$ but, again, this was not paid attention to.[40] All works coincide in two observations when these oxides are studied at low $pO_2$: as x increases the amount of oxygen vacancies increases very fast and the electric conductivity decreases. It has also been observed that the increase of oxygen vacancies is correlated with a higher lattice expansion as $pO_2$ reduces.[41]

Nevertheless, we have not found in the literature an explanation of why the formation of vacancies increases much faster on heavily doped oxide perovskites although this is important for the final electrical behavior. As an explanation, we have to rule out lattice effects coming from A-site mean ionic radii or the A-site disorder because this occurs either with them fixed (present case) and when they are left to change for every x-value (all other examples). The synthesis method seems not to be an option either because all show the same behavior (present case and in the literature). There is a correlation with the reduction of the lattice volume but it is difficult to find cause-effect relationship in this case considering that the lattice expansion, bigger for higher x, seems to override this effect at low $pO_2$ as indicated before[41]. What is common in all cases, including the present, is the reduction of the mean electronegativity of the A-site cations, which is systematically reduced as calcium or strontium ions substitute the more electronegative rare earths[42]. The lowering of the average electronegativity of the A-site with x might facilitate the creation of oxygen vacancies and, as a result, the reduction of conductivity is bigger in the most heavily

doped oxides. At sufficiently low oxygen partial pressure this greater reduction for samples with higher x leads to an inversion of the tendency with doping: conductivity reduces with doping instead of increasing.

We consider that this is an interesting finding because most studies are focused, including this one, on finding the highest conductivity of a group of oxide perovskites by increasing the doping but if the conductivity is not tested at sufficiently low oxygen partial pressures (present case is ~$10^{-21}$ atm), the observed results might not be representative of the final behavior under SOFC operation conditions as this study shows.

*3.4. Thermal expansion study*

Thermal expansion measurements on rectangular bars carried out in air atmosphere upon heating from 200 to 950ºC are shown in Figure 9a-c. The average linear thermal expansion coefficient obtained from this figure for each sample is shown in Figure 9d.

Figure 9

It can be seen that, although the thermal expansion coefficients (TEC) of all phases are all very similar and also agree with those of similar chromite perovskites[43], there is a small increase in TECs with increasing the doping level x in the three families of perovskites prepared.

This increase may be attributed to the formation of oxygen vacancies and the concomitant reduction of $Cr^{4+}$ and $Ni^{3+}$ ions with increasing x as both processes will result in lattice expansion. It is interesting to note that the TEC values obtained for the samples with low amount of dopant are very close to those of YSZ electrolyte ($TEC_{(8YSZ;300\text{-}1000ºC)}$ = 10.0-10.8x$10^{-6}$ $K^{-1}$) [44], and those are also the phases with higher

conductivity, which is quite important if these oxides were to be used as anodes. The higher expansion of the most heavily doped phases agrees with all the literature data: either under air or under low $pO_2$ atmosphere it is always observed that lattice expansion increases with temperature due to the increase of oxygen vacancies and, as indicated previously, given that the amount of vacancies formed increases with x, the same is expected to occur with the thermal expansion coefficients.

## 4. Conclusions

A series of perovskites with the general formula $Ln_{1-x}M_xCr_{0.9}Ni_{0.1}O_3$ (Ln=La and/or Nd; M=Sr and/or Ca; $x \leq 0.25$) has been prepared by the combustion method using glycine, urea and sucrose as fuels. The effect of doping x has been isolated from other lattice effects by fixing $\langle r_A \rangle$ to 1.22 Å and $\sigma^2(r_A)$ to 0.0001 $Å^2$. At room temperature, all compounds show orthorhombic symmetry (S.G: *Pnma*) and the unit cell compresses as x increases. There is also a systematic increase in grain growth with doping, which is consistent with the introduction of increasing amounts of alkaline-earth cation, specially Ca, which is believe to form low temperature melting intermediate species that promote sintering.

The electrical conductivity measured in $H_2$ shows important dependences with x and with the synthetic method. Irrespective of x, conductivity is always higher in the following order: urea, glycine and sucrose. An interesting observation is that, upon doping, the electronic conductivity measured under hydrogen atmosphere decreases contrary to common expectations for a p-type doping of the oxide perovskites. This effect has not been reported before although there were some evidences that this could occur under reducing conditions at sufficiently low oxygen partial pressures. Moreover,

this behaviour is consistent with all literature works that report the increase of oxygen vacancy formation with x, which could be attributed to the lower charge density of the doping cations. As a consequence, only samples with lower doping values have conductivity values that are reasonable for a SOFC anode. Thermal expansion coefficients are also closer to that of the most common SOFC electrolyte (YSZ) for samples with lower x, which indicates that less doped phases are the only ones that reasonably meet the basic needs as anodes.



**Acknowledgements**

This research has been funded by the Ministerio de Economía y Competitividad (MAT2016-76739-R), the Feder program of the European Union and Dpto. Educación, Política Lingüística y Cultura of the Basque Goverment (IT-630-13). The authors thank for technical and human support provided by SGIker of UPV/EHU. L.Ortega-San-Martin acknowledges Departamento de Ciencias, PUCP (Peru), for funding two shorts stays at UPV/EHU.

**References**

[1] N. Mahato, A. Banerjee, A. Gupta, S. Omar, K. Balani, Progress in material selection for solid oxide fuel cell technology: A review, Prog. Mater. Sci. 72 (2015) 141–337. doi:10.1016/j.pmatsci.2015.01.001.

[2] W.-H. Kan, V. Thangadurai, Challenges and prospects of anodes for solid oxide fuel cells (SOFCs), Ionics (Kiel). 21 (2014) 301–318. doi:10.1007/s11581-014-1334-6.

[3] D.K. Niakolas, Sulfur poisoning of Ni-based anodes for Solid Oxide Fuel Cells in H/C-based fuels, Appl. Catal. A Gen. 486 (2014) 123–142. doi:10.1016/j.apcata.2014.08.015.

[4] J.T.S. Irvine, Perovskite Oxide for Solid Oxide Fuel Cells, in: T. Ishihara (Ed.), Perovskite Oxide Solid Oxide Fuel Cells, Springer Science, 2009: pp. 167–182.

doi:10.1007/978-0-387-77708-5.

[5] S. Tao, J.T.S. Irvine, Discovery and characterization of novel oxide anodes for solid oxide fuel cells, Chem. Rec. 4 (2004) 83–95. doi:10.1002/tcr.20003.

[6] N.P. Brandon, S. Skinner, B.C.H. Steele, Recent Advances in Materials for Fuel Cells, Annu. Rev. Mater. Res. 33 (2003) 183–213. doi:10.1146/annurev.matsci.33.022802.094122.

[7] I.Z. Rahman, M.A. Raza, M.A. Rahman, Perovskite Based Anode Materials for Solid Oxide Fuel Cell Application: A Review, Adv. Mater. Res. 445 (2012) 497–502. doi:10.4028/www.scientific.net/AMR.445.497.

[8] S. Gupta, H. Sabarou, Y. Zhong, P. Singh, Phase evolution and electrochemical performance of iron doped lanthanum strontium chromite in oxidizing and reducing atmosphere, Int. J. Hydrogen Energy. 42 (2017) 6262–6271. doi:10.1016/j.ijhydene.2016.11.141.

[9] H. Teruhisa, Perovskite Oxide for Solid Oxide Fuel Cells, in: Perovskite Oxide Solid Oxide Fuel Cells, 2009: pp. 285–296. doi:10.1007/978-0-387-77708-5.

[10] J. Sfeir, LaCrO3-based anodes: Stability considerations, J. Power Sources. 118 (2003) 276–285. doi:10.1016/S0378-7753(03)00099-5.

[11] O. V. Komova, V.I. Simagina, S.A. Mukha, O. V. Netskina, G. V. Odegova, O.A. Bulavchenko, A. V. Ishchenko, A.A. Pochtar', A modified glycine-nitrate combustion method for one-step synthesis of LaFeO3, Adv. Powder Technol. 27 (2016) 496–503. doi:10.1016/j.apt.2016.01.030.

[12] S. Singh, D. Singh, LaSrFeO4 nanopowders synthesized by different combustion methods: Effect of fuel/particle size, Ceram. Int. 42 (2016) 15725–15731. doi:10.1016/j.ceramint.2016.07.032.

[13] D.P. Tarragó, C. de F. Malfatti, V.C. de Sousa, Influence of fuel on morphology of LSM powders obtained by solution combustion synthesis, Powder Technol. 269 (2015) 481–487. doi:10.1016/j.powtec.2014.09.037.

[14] F. Deganello, L.F. Liotta, G. Marcì, E. Fabbri, E. Traversa, Strontium and iron-doped barium cobaltite prepared by solution combustion synthesis: exploring a mixed-fuel approach for tailored intermediate temperature solid oxide fuel cell cathode materials, Mater. Renew. Sustain. Energy. 2 (2013) 8. doi:10.1007/s40243-013-0008-z.

[15] L.M. Rodriguez-Martinez, J.P. Attfield, Cation disorder and size effects in magnetoresistive manganese oxide perovskites, Phys. Rev. B. 54 (1996)

R15622–R15625.

[16] A.K. Kundu, M.M. Seikh, K. Ramesha, C.N.R. Rao, Novel effects of size disorder on the electronic and magnetic properties of rare earth manganates of the type La 0.7− x Ln x Ba 0.3 MnO 3 (Ln = Pr,Nd, Gd or Dy) with large average radius of the A-site cations, J. Phys. Condens. Matter. 17 (2005) 4171–4180. doi:10.1088/0953-8984/17/26/015.

[17] K. Vidal, A. Larrañaga, A. Morán-Ruiz, A.T. Aguayo, M.A. Laguna-Bercero, M.P. Yeste, J.J. Calvino, M.I. Arriortua, Effect of synthesis conditions on electrical and catalytical properties of perovskites with high value of A-site cation size mismatch, Int. J. Hydrogen Energy. 41 (2016) 19810–19818. doi:10.1016/j.ijhydene.2016.02.088.

[18] J.-G. Cheng, J.-S. Zhou, J.B. Goodenough, Lattice effects on ferromagnetism in perovskite ruthenates., Proc. Natl. Acad. Sci. U. S. A. 110 (2013) 13312–5. doi:10.1073/pnas.1311871110.

[19] A. Ecija, K. Vidal, A. Larrañaga, A. Martínez-Amesti, L. Ortega-San-Martín, M.I. Arriortua, Structure and properties of perovskites for SOFC cathodes as a function of the A-site cation size disorder, Solid State Ionics. 235 (2013) 14–21. doi:https://doi.org/10.1016/j.ssi.2013.01.010.

[20] Larson A. C., R.B. Von Dreele, General Structure Analysis System (GSAS), Los Alamos Lab. Rep. LAUR 86-74 (2004).

[21] B.H. Toby, EXPGUI, a graphical user interface for GSAS, J. Appl. Crystallogr. 34 (2001) 210–213. doi:10.1107/S0021889801002242.

[22] K. Oikawa, T. Kamiyama, T. Hashimoto, Y. Shimojyo, Y. Morii, Structural Phase Transition of Orthorhombic LaCrO3 Studied by Neutron Powder Diffraction, J. Solid State Chem. 154 (2000) 524–529. doi:10.1006/jssc.2000.8873.

[23] L. Ortega-San-Martín, K. Vidal, B. Roldán-Pozo, Y. Coello, A. Larrañaga, M.I. Arriortua, Synthesis method dependence of the lattice effects in Ln 0.5 M 0.5 FeO 3 perovskites (Ln = La and (Nd or Gd); M = Ba and (Ca or Sr)), Mater. Res. Express. 3 (2016) 56302. doi:10.1088/2053-1591/3/5/056302.

[24] R.D. Shannon, Revised Effective Ionic Radii and Systematic Studies of Interatomie Distances in Halides and Chaleogenides, Acta Cryst. A32 (1976) 751–767. doi:10.1107/S0567739476001551.

[25] A.L.A. Da Silva, G.G.G. Castro, M.M.V.M. Souza, Synthesis of Sr-doped LaCrO

3 powders by combustion method: Influence of the fuel agent, J. Therm. Anal. Calorim. 109 (2012) 33–38. doi:10.1007/s10973-011-1527-4.

[26] B.S. Barros, J. Kulesza, D.M. De Arajo Melo, A. Kiennemand, Nickel-based catalyst precursor prepared via microwave-induced combustion method: Thermodynamics of synthesis and performance in dry reforming of CH4, Mater. Res. 18 (2015) 732–739. doi:10.1590/1516-1439.018115.

[27] S. Simner, J. Hardy, J. Stevenson, T. Armstrong, Sintering mechanisms in strontium doped lanthanum chromite, J. Mater. Sci. 34 (1999) 5721–5732. doi:10.1023/A:1006733414271.

[28] S.W. Paulik, S. Baskaran, T.R. Armstrong, Mechanical properties of calcium- and strontium- substituted lanthanum chromite, J. Mater. Sci. 3 (1998) 2397–2404.

[29] S.R. Nair, R.D. Purohit, A.K. Tyagi, P.K. Sinha, B.P. Sharma, Role of glycine-to-nitrate ratio in influencing the powder characteristics of La(Ca)CrO3, Mater. Res. Bull. 43 (2008) 1573–1582. doi:10.1016/j.materresbull.2007.06.021.

[30] I. Yasuda, T. Hikita, Electrical Conductivity and Defect Structure of Calcium-Doped Lanthanum Chromites, J. Electrochem. Soc. 140 (1993) 1699. doi:10.1149/1.2221626.

[31] I. Yasuda, M. Hishinuma, Electrical conductivity and chemical diffusion coefficient of Sr-doped lanthanum chromites, Solid State Ionics. 80 (1995) 141–150. doi:http://dx.doi.org/10.1016/0167-2738(95)00136-T.

[32] S. Tao, J.T.S. Irvine, Structural and electrochemical properties of the perovskite oxide Pr0.7Sr0.3Cr0.9Ni0.1O3 − δ, Solid State Ionics. 179 (2008) 725–731. doi:https://doi.org/10.1016/j.ssi.2008.04.027.

[33] S. Tao, J.T.S. Irvine, Phase Transition in Perovskite Oxide La0.75Sr0.25Cr0.5Mn0.5O3-δ Observed by in Situ High-Temperature Neutron Powder Diffraction, Chem. Mater. 18 (2006) 5453–5460. doi:10.1021/cm061413n.

[34] J.T.S. Irvine, P. Connor, Alternative Materials for SOFCs, Opportunities and limitations, in: J.T.S. Irvine, P. Connor (Eds.), Solid Oxide Fuels Cells Facts Fig. Past, Present Futur. Perspect. SOFC Technol., Springer-Verlag, London, 2013: pp. 163–180. doi:10.1007/978-1-4471-4456-4_7.

[35] D.P. Karim, A.T. Aldred, Localized level hopping transport in La(Sr)CrO3, Phys. Rev. B. 20 (1979) 2255–2263. doi:10.1103/PhysRevB.20.2255.

[36] S.P. Jiang, L. Liu, K.P. Ong, P. Wu, J. Li, J. Pu, Electrical conductivity and performance of doped LaCrO3 perovskite oxides for solid oxide fuel cells, J. Power Sources. 176 (2008) 82–89. doi:10.1016/j.jpowsour.2007.10.053.

[37] N. Sakai, T. Kawada, H. Yokokawa, M. Dokiya, T. Iwata, Sinterability and electrical conductivity of calcium-doped lanthanum chromites, J. Mater. Sci. 25 (1990) 4531–4534. doi:10.1007/BF00581119.

[38] L. Manxi, C. Xiangfeng, Z. Weichang, D. Yongping, C. Tongyun, Preparation and Performance of Sm1-xCaxCrO3-δ as New Interconnect Materials for IT-SOFC, Rare Met. Mater. Eng. 43 (2014) 1337–1341. doi:10.1016/S1875-5372(14)60119-3.

[39] K.J. Yoon, C.N. Cramer, E.C. Thomsen, C.A. Coyle, G.W. Coffey, O.A. Marina, Calcium- and Cobalt-Doped Yttrium Chromites as an Interconnect Material for Solid Oxide Fuel Cells, J. Electrochem. Soc. 157 (2010) B856–B861. doi:10.1149/1.3337156.

[40] A.S. Mukasyan, C. Costello, K.P. Sherlock, D. Lafarga, A. Varma, Perovskite membranes by aqueous combustion synthesis: Synthesis and properties, Sep. Purif. Technol. 25 (2001) 117–126. doi:10.1016/S1383-5866(01)00096-X.

[41] F. Boroomand, E. Wessel, H. Bausinger, K. Hilpert, Correlation between defect chemistry and expansion during reduction of doped LaCrO3 interconnects for SOFCs, Solid State Ionics. 129 (2000) 251–258. doi:10.1016/S0167-2738(99)00330-6.

[42] J.E. Huheey, E.A. Keiter, R.L. Keiter, Inorganic Chemistry. Principles of Structure and Reactivity, 4th Editio, Harper Collins College Publishers, New York, 1993.

[43] M.K. Rath, K.T. Lee, Investigation of aliovalent transition metal doped La0.7Ca0.3Cr0.8X0.2O3-δ (X=Ti, Mn, Fe, Co, and Ni) as electrode materials for symmetric solid oxide fuel cells, Ceram. Int. 41 (2015) 10878–10890. doi:10.1016/j.ceramint.2015.05.029.

[44] V. V. Kharton, F.M.B. Marques, A. Atkinson, Transport properties of solid oxide electrolyte ceramics: A brief review, Solid State Ionics. 174 (2004) 135–149. doi:10.1016/j.ssi.2004.06.015.

## TABLES and table captions

Table 1. Nominal stoichiometries of $Ln_{1-x}M_xCr_{0.9}Ni_{0.1}O_3$ perovskites.

| x | $Ln_{1-x}M_xCr_{0.9}Ni_{0.1}O_3$ | $<r_A>$ (Å) | $\sigma^2(r_A)$ (Å$^2$) |
|---|---|---|---|
| 0.10 | $La_{0.85}Nd_{0.05}Sr_{0.10}Cr_{0.90}Ni_{0.10}O_3$ | 1.22 | 0.00010 |
| 0.15 | $La_{0.80}Nd_{0.05}Sr_{0.10}Ca_{0.05}Cr_{0.90}Ni_{0.10}O_3$ | 1.22 | 0.00011 |
| 0.20 | $La_{0.80}Sr_{0.10}Ca_{0.10}Cr_{0.90}Ni_{0.10}O_3$ | 1.22 | 0.00011 |
| 0.25 | $La_{0.75}Sr_{0.10}Ca_{0.15}Cr_{0.90}Ni_{0.10}O_3$ | 1.22 | 0.00011 |

Table 2. Summary of the ICP results for the $Ln_{1-x}M_xCr_{0.9}Ni_{0.1}O_3$ perovskites.

| x | Fuel | $Ln_{1-x}M_xCr_{0.9}Ni_{0.1}O_3$ |
|---|---|---|
| 0.10 | Glycine | $La_{0.86(1)}Nd_{0.04(1)}Sr_{0.11(1)}Cr_{0.90(2)}Ni_{0.10(1)}$ |
| | Urea | $La_{0.87(1)}Nd_{0.05(1)}Sr_{0.10(1)}Cr_{0.90(2)}Ni_{0.11(1)}$ |
| | Sucrose | $La_{0.85(1)}Nd_{0.05(1)}Sr_{0.11(1)}Cr_{0.90(2)}Ni_{0.11(1)}$ |
| 0.15 | Glycine | $La_{0.76(1)}Nd_{0.04(1)}Sr_{0.11(1)}Ca_{0.07(1)}Cr_{0.90(1)}Ni_{0.10(1)}$ |
| | Urea | $La_{0.78(1)}Nd_{0.05(1)}Sr_{0.10(1)}Ca_{0.05(1)}Cr_{0.90(1)}Ni_{0.10(1)}$ |
| | Sucrose | $La_{0.81(1)}Nd_{0.06(1)}Sr_{0.10(1)}Ca_{0.06(1)}Cr_{0.90(1)}Ni_{0.10(1)}$ |
| 0.20 | Glycine | $La_{0.82(1)}Sr_{0.10(1)}Ca_{0.09(1)}Cr_{0.90(2)}Ni_{0.10(1)}$ |
| | Urea | $La_{0.80(1)}Sr_{0.10(1)}Ca_{0.11(1)}Cr_{0.90(2)}Ni_{0.10(1)}$ |
| | Sucrose | $La_{0.81(1)}Sr_{0.11(1)}Ca_{0.10(1)}Cr_{0.90(2)}Ni_{0.11(1)}$ |
| 0.25 | Glycine | $La_{0.74(1)}Sr_{0.08(2)}Ca_{0.16(1)}Cr_{0.90(2)}Ni_{0.11(1)}$ |
| | Urea | $La_{0.75(1)}Sr_{0.09(2)}Ca_{0.15(1)}Cr_{0.90(2)}Ni_{0.10(1)}$ |
| | Sucrose | $La_{0.75(1)}Sr_{0.11(1)}Ca_{0.13(1)}Cr_{0.89(2)}Ni_{0.10(1)}$ |



## Figure Captions

Figure 1. X-ray diffraction patterns for the series $Ln_{1-x}M_xCr_{0.9}Ni_{0.1}O_3$ (Ln = La and/or Nd; M = Sr and/or Ca; $x \leq 0.25$) prepared using (a) glycine, (b) urea and (c) sucrose as fuel agents.

Figure 2. Rietveld fits to the powder XRD data using orthorhombic *Pnma* space group for the compounds obtained using urea as fuel.

Figure 3. Variation of the unit cell parameters and volume with doping for the samples obtained using different fuels. Lines are linear fits in all cases.

Figure 4. Comparison of the XRD data taken for x=0.1 phase under different atmosphere conditions: as –synthesised, after $H_2$-conductivity test and after reoxidation in air.

Figure 5. SEM micrographs of $Ln_{1-x}M_xCr_{0.9}Ni_{0.1}O_3$ perovskites calcined between 1100 and 1200ºC.

Figure 6. SEM micrographs taken on the surface of the pellets sintered at 1350ºC in air for 10 h.

Figure 7. Doping and fuel dependence of the average particle sizes calculated from SEM images.

Figure 8. Conductivity dependence upon temperature as a function of x measured in $H_2$ for the oxides prepared using (a) glycine, (b) urea and (c) sucrose as fuel agents. Oxides were previously sintered at 1350ºC in air for 10 h. The evolution of the conductivity with x at 800ºC is shown in (d). Lines are guides for the eyes.

Figure 9. Thermal expansion behaviour of $Ln_{1-x}M_xCr_{0.9}Ni_{0.1}O_3$ perovskites obtained using (a) glycine, (b) urea and (c) sucrose as fuels and sintered at 1350ºC in air for 10 h. The evolution of the thermal expansion coefficients with x is shown in (d).

Figure 1.

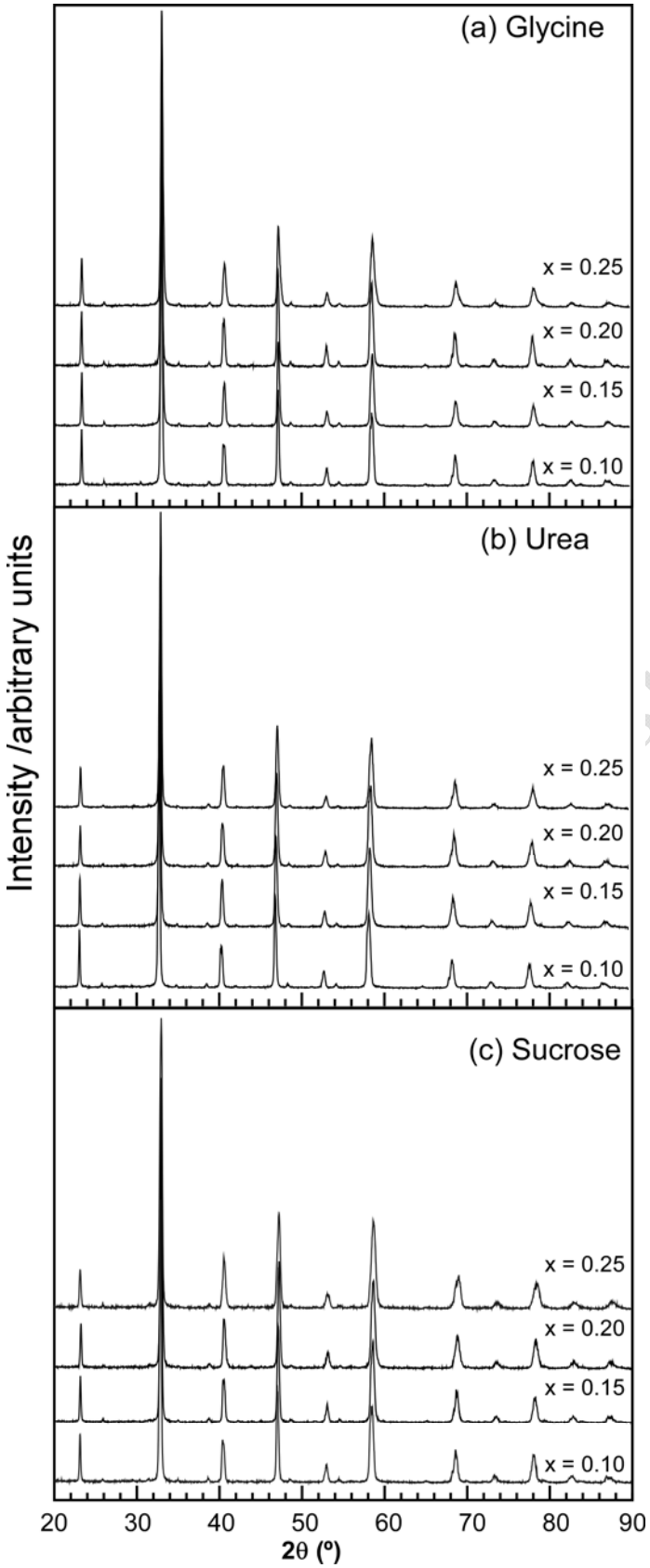

Figure 2

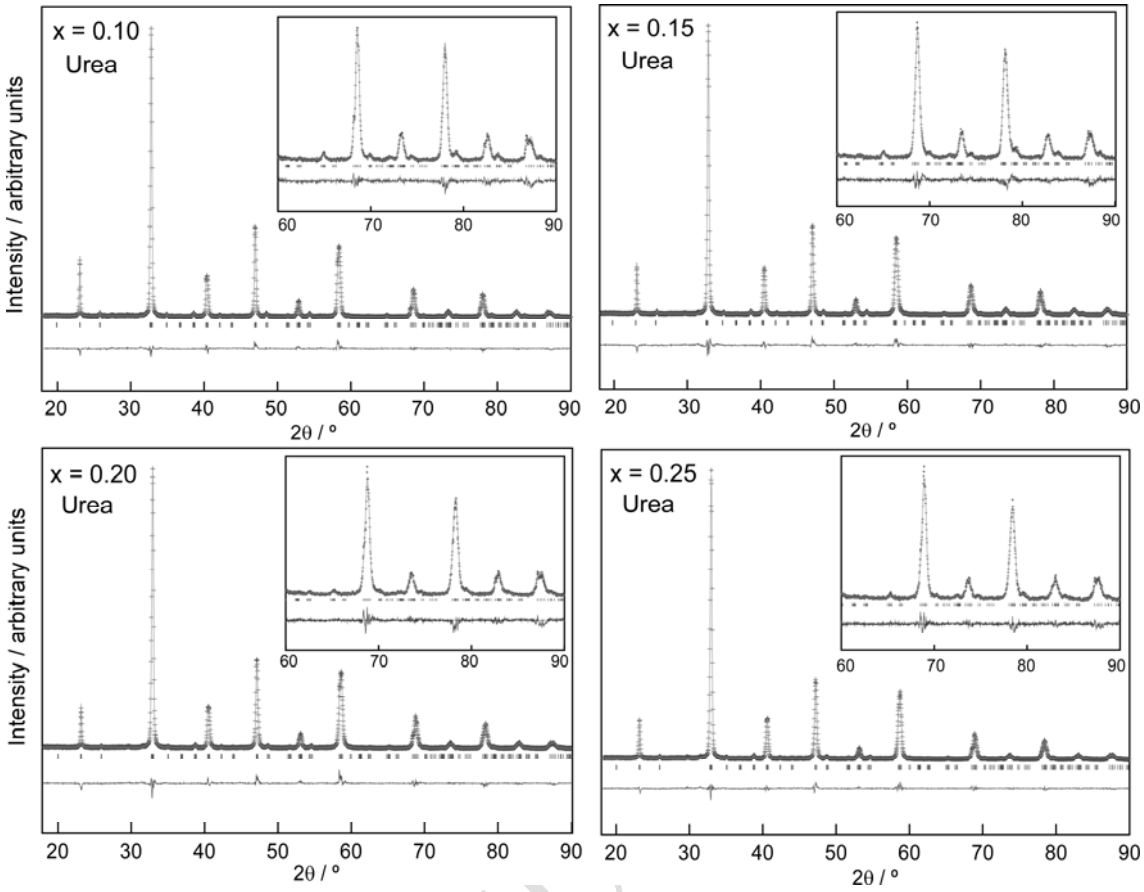


Figure 3.

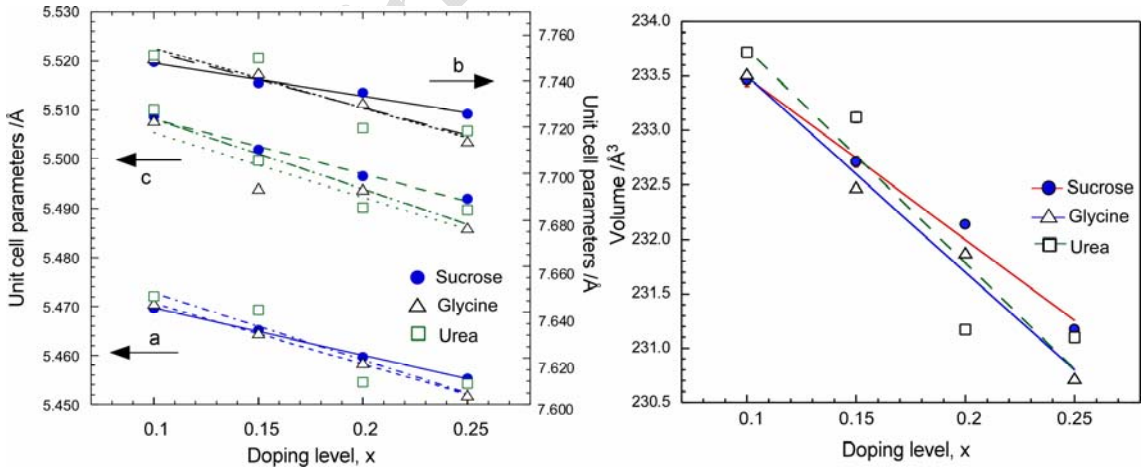

Figure 4

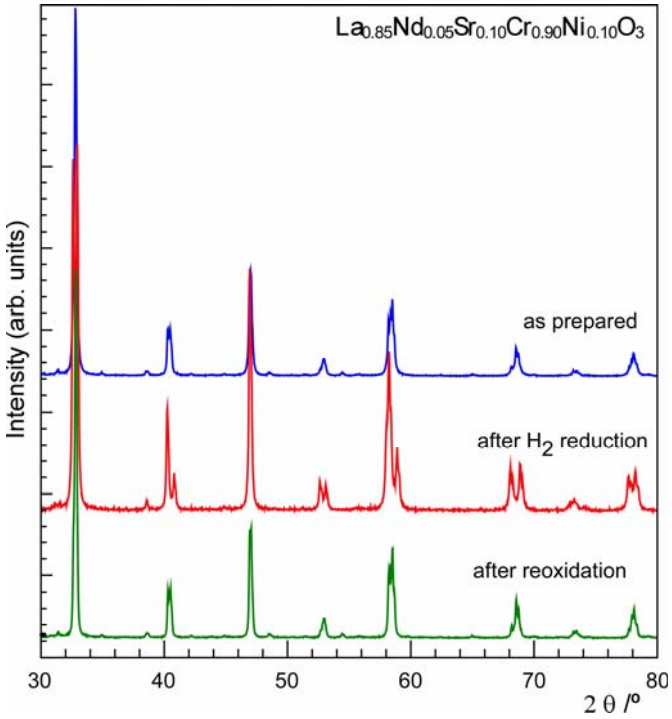


Figure 5

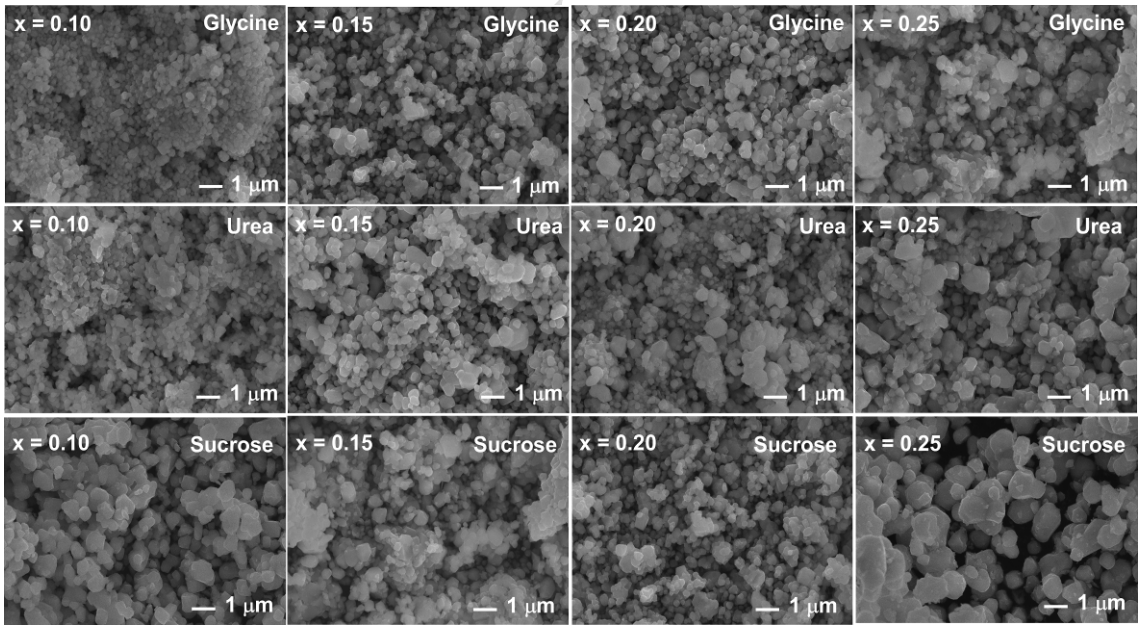

Figure 6

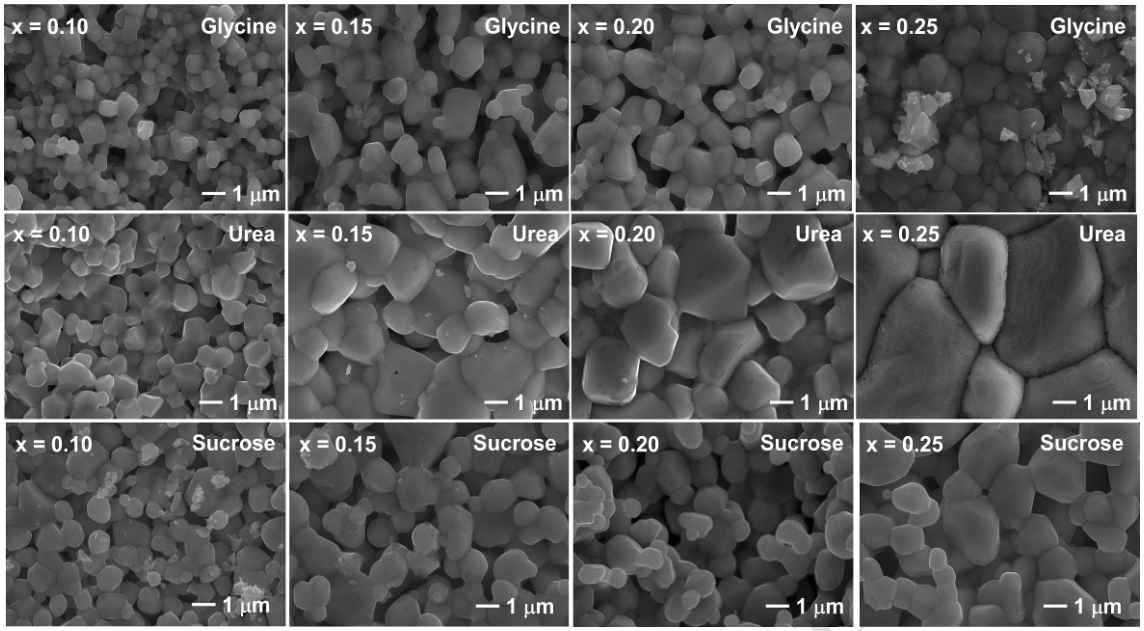


Figure 7

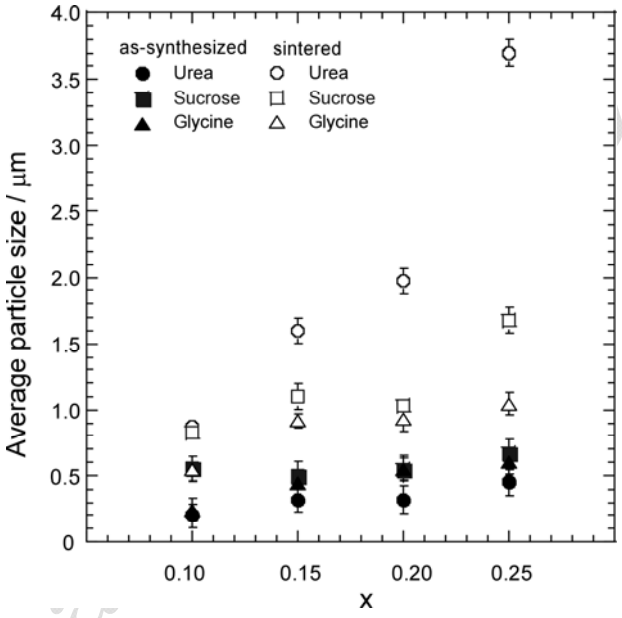

Figure 8

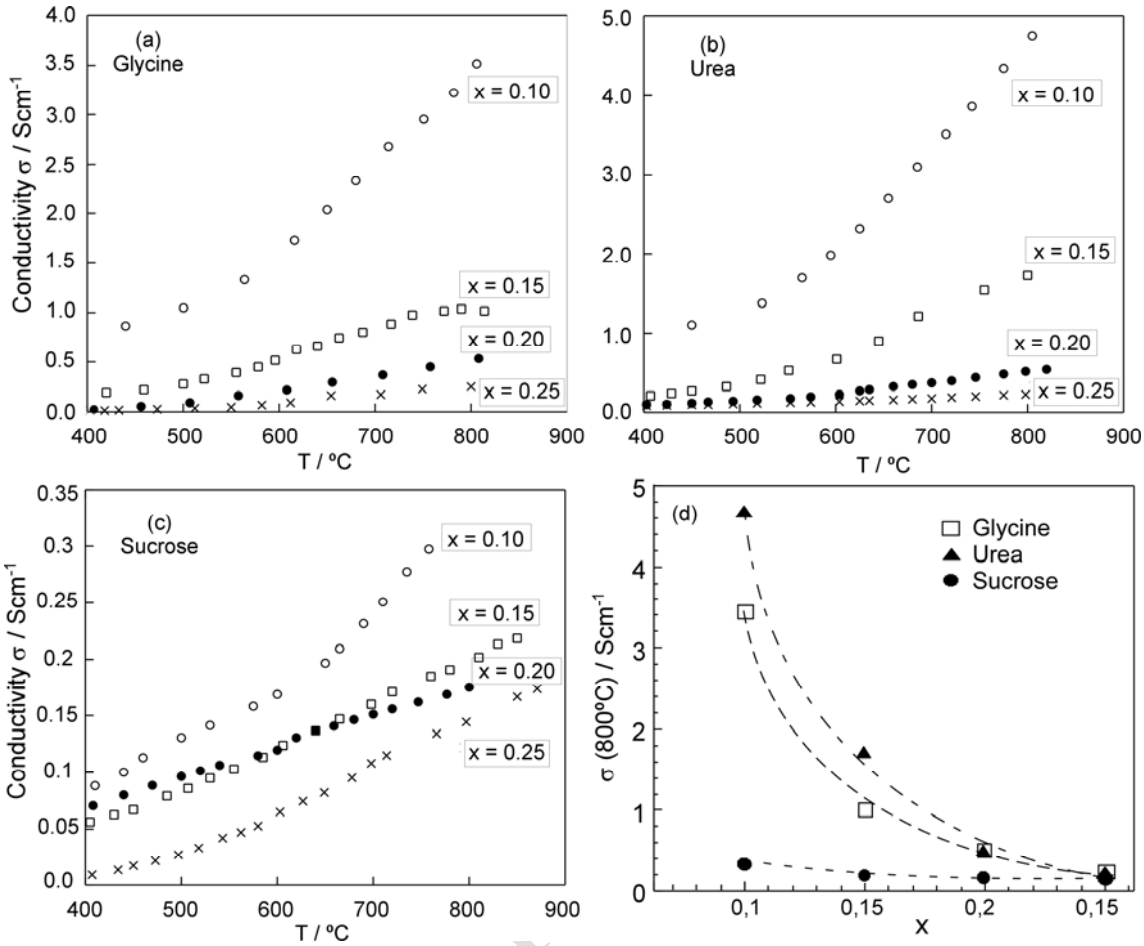

Figure 9